Dynamic intermolecular interactions control adsorption from mixtures of natural organic matter and protein onto titanium dioxide nanoparticles

Sheyda Shakiba,[1] Alireza Hakimian,[1] Luis R. Barco,[1] and Stacey M. Louie[1,*]

[1]Department of Civil and Environmental Engineering,

University of Houston, Houston, Texas 77204, United States

[*]Corresponding author:

Phone: 713-743-8646

Fax: 713-743-4260

Email: slouie@uh.edu

Word Count: 5499 text + (5 figures)*300 = 6999 words

TABLE OF CONTENTS FIGURE

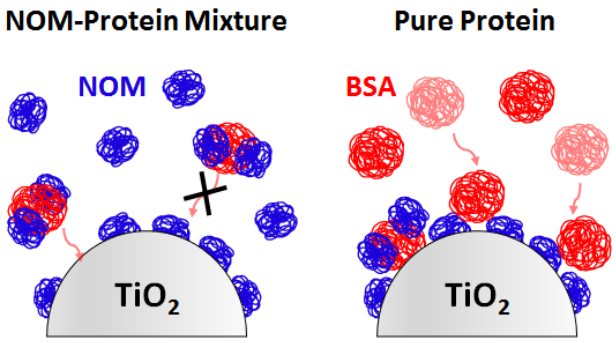

Abstract

Engineered nanoparticles (NPs) will obtain macromolecular coatings in environmental systems, changing their subsequent interactions. The matrix complexity inherent in natural waters and wastewaters greatly complicates prediction of the corona formation. Here, we investigate corona formation on titanium dioxide (TiO_2) NPs from mixtures of natural organic matter (NOM) and a protein, bovine serum albumin (BSA), to thoroughly probe the role of mixture interactions in the adsorption process. Fundamentally different coronas were observed under different NP exposure conditions and time scales. In mixtures of NOM and protein, the corona composition was kinetically determined, and the species initially co-adsorbed but were ultimately limited to monolayers. On the contrary, sequential exposure of the NPs to pure solutions of NOM and protein resulted in extensive multilayer formation. The intermolecular complexation between NOM and BSA in solution and at the NP surface was the key mechanism controlling these distinctive adsorption behaviors, as determined by size exclusion chromatography (SEC) and *in situ* attenuated total reflectance – Fourier transform infrared (ATR-FTIR) spectroscopy. Overall, this study demonstrates that dynamic intermolecular interactions and the history of the NP surface must be considered together to predict corona formation on NPs in complex environmental media.

Introduction

Engineered nanoparticles (NPs) have gained attention for applications in myriad fields such as water treatment and drug delivery, while concerns for potential environmental risks have also arisen.[1-3] The adsorption of macromolecules to form a coating or corona on the NP surface significantly changes the environmental fate and biological interactions of the NPs,[4-17] and hence surface chemistry is a critical property of the NP. In complex matrices, the corona composition is difficult to characterize or predict. For example, natural organic matter (NOM) or humic substances can show adsorptive fractionation, such that the composition of the adsorbed layer differs from that of the bulk solution,[18-24] and extensive studies on protein corona formation in physiological media have highlighted the dynamic nature of the adsorption process.[12-17] To our knowledge, few studies are available for NPs in environmental media comprising multiple classes of macromolecules, including not only NOM but also proteins, polysaccharides, and other biomolecules.[25, 26] This research gap contributes uncertainty in interpreting NP behavior in complex environmental matrices, when the ultimate NP surface composition is unknown.

Here, we investigate the competitive adsorption of NOM and a protein, bovine serum albumin (BSA), onto titanium dioxide (TiO_2) NPs as a model system to identify the mechanisms controlling corona formation on NPs in complex environmental mixtures. TiO_2 NPs are photoreactive and hence of interest for water treatment applications,[27-31] but surface fouling (or corona formation) can modify the effectiveness of the NPs.[32-34] Our long-term goal is to predict the photoreactivity of TiO_2 in complex media. To do so first requires a thorough understanding of the corona formation. To our knowledge, only single-component adsorption of NOM[35-38] or BSA[37, 39-41] onto TiO_2 NPs has previously been evaluated. Adsorption of NOM and protein together has primarily been studied in the soil sciences, where zonal organic matter structures proposed by

Kleber et al.[42] were attributed in part to multilayers that form upon sequential adsorption of pure proteins over NOM coatings on mineral surfaces.[43-45] However, in these studies, the influence of solution-phase interactions that can occur between NOM and protein (prior to adsorption) has not yet been fully explored. A recent study by Schmidt et al. identified that solution-phase complexation of BSA onto DNA reduces repulsive interactions to enhance DNA adsorption to goethite surfaces.[46] As proteins also complex with NOM,[47-53] we hypothesize that complexation can influence adsorption from mixtures of NOM and protein onto NPs. A comprehensive understanding of the adsorption process must therefore consider all possible interactions between NOM, protein, and TiO_2 NPs, including those between the uncoated NPs and macromolecules, between NOM and protein in solution (e.g., complexation[48-52]), and between adsorbed and dissolved macromolecules (e.g., displacement[54-56] or multi-layer adsorption[43-45]).

The objective of this study is to achieve a mechanistic understanding of the fundamental processes controlling the adsorption of mixtures of NOM and BSA onto TiO_2 NPs, by investigating solution and surface interactions, as well as the kinetics and history of these interactions. Batch adsorption experiments were evaluated against theoretical equilibrium and kinetic adsorption models. We then focus on the influence of NOM-protein complexation on the adsorption process, using size exclusion chromatography (SEC) to identify complexation and *in situ* attenuated total reflectance – Fourier transform infrared (ATR-FTIR) spectroscopy to probe competitive adsorption, co-adsorption, or multilayer adsorption phenomena under different NP exposure conditions. We expect this fundamental knowledge will be useful to identify the range of processes that can affect corona formation on NPs in complex environmental media.

Materials and methods

Materials

TiO_2 NPs (Standard Reference Material (SRM) 1898) were obtained from the National Institute of Standards and Technology (NIST, Gaithersburg, MD), Suwannee River NOM (Cat. No. 1R101N) from the International Humic Substances Society (IHSS, St. Paul, MN), and bovine serum albumin (BSA, reagent grade pure powder) from Sera Care Life Sciences (Milford, MA). Other reagents are specified in the Supporting Information (SI). BSA (1 g L^{-1}) and NOM (1 g L^{-1}) stock solutions were prepared in Milli-Q water, adjusted to pH 7 using (0.1 or 1) M HCl or NaOH, and allowed to equilibrate overnight to dissolve. Stock solutions were filtered through 0.22 μm polyethersulfone membranes (EMD Millipore, Burlington, MA). Filter loss (to correct subsequent concentrations) was determined against unfiltered stocks for BSA by absorbance at 280 nm on a UV-2600 spectrophotometer (Shimadzu, Columbia, MD) (< 5% filter loss), and for NOM by total organic carbon (TOC) analysis (Xenco Laboratories, Houston, TX) or SEC with refractive index (RI) detection, described in the SI (8% to 10% filter loss). Subsequent samples containing NOM or BSA were prepared in an aqueous buffer of 1.2 mM $NaHCO_3$ and 0.85 mM $CaCl_2$ (pH 7 to 7.5), representing a simplified Environmental Protection Agency (EPA) moderately hard water[57] (matching the total monovalent and divalent cation concentrations using only $NaHCO_3$ and $CaCl_2$), and provides similar pH, bicarbonate, and calcium concentrations to those reported in freshwater systems.[58]

Preparation and characterization of TiO_2 suspensions

Stock suspensions of TiO_2 NPs (2 g L^{-1} in Milli-Q water) were dispersed using an ultrasonication probe (TM250B Tekmar Sonic Disruptor, Cincinnati, OH) at a measured power[59] of (20 ± 3) W for three 5-min intervals, immediately prior to use. The NPs have reported crystallite particle diameters of (19 ± 2) nm for anatase (comprising 76% of the sample) and (37 ± 6) nm for rutile (comprising 24%).[60] Dynamic light scattering (DLS) measurements (Zetasizer Nano, Malvern Instruments, Westborough, MA) were taken to determine the hydrodynamic size as the *z*-average diameter of (155 ± 11) nm, intensity-average diameter of (182 ± 14) nm, or volume-average diameter of (118 ± 8) nm for stock suspensions diluted to 0.2 g L^{-1} TiO_2 NPs in 1 mM NaCl (pH 5.6 ± 0.5), confirming good dispersion of the NPs compared to the reported volume-mean diameter in the NIST SRM 1898 Certificate of Analysis (CoA).[60] After each adsorption experiment, DLS size was also measured directly on samples containing 0.5 g L^{-1} NPs in the buffer stated above. A specific surface area of 54 m^2 g^{-1} reported in the NIST CoA (from Brunauer–Emmett–Teller (BET) analysis) was used to calculate adsorbed masses.

Characterization of BSA and NOM solutions by SEC

Solutions of BSA and NOM and their mixtures were prepared in the $CaCl_2$/$NaHCO_3$ medium noted above, fixing one species' concentration at 100 mg L^{-1} and varying the other from (10 to 200) mg L^{-1}. SEC analysis was performed using a Superdex 75 10/300 GL analytical SEC column (GE Healthcare, Chicago, Illinois) on an Agilent 1290 Infinity system comprising a binary pump, degasser, and autosampler (Agilent, Santa Clara, CA). 100 µL of sample was injected. The eluent was 4 mM phosphate (pH 7) with 25 mM NaCl at a flow rate of 0.7 mL min^{-1}.[61 62] Similar results were observed in eluent matching the sample buffer (Figure S2), but column fouling by

NOM occurred in Ca^{2+}-containing media. A UV-vis diode array detector (Agilent 1260 UV-DAD), fluorescence detector (Agilent 1260 FLD), and refractive index (RI) detector (Wyatt, Optilab T-rEX) were situated in-line after the SEC column. The DAD monitored absorbance across (200 to 500) nm in 2 nm increments. The FLD monitored the fluorescence of BSA at excitation/emission wavelengths of (295/345) nm.[63] Complexation of NOM onto BSA was evaluated within 1 h of mixing, based on the change in UV and FLD peak areas across the BSA elution time and depletion in RI peak area across the NOM elution time, on duplicate samples. The complexation kinetics of BSA (100 mg L^{-1}) and NOM (100 mg L^{-1}) were also evaluated.

Batch adsorption isotherms

Adsorption isotherms onto TiO_2 NPs (0.5 g L^{-1}) were obtained in triplicate. Single-component isotherms were collected for initial concentrations of BSA from (60 to 250) mg L^{-1} or NOM from (10 to 200) mg L^{-1} in the $CaCl_2$/$NaHCO_3$ buffer. The buffer and adsorbates were mixed, followed by NP addition within 1 h. Samples were covered with aluminum foil and rotated end-over-end at 25 rpm at room temperature for approximately 24 h. Then, 1.5 mL of sample was centrifuged in an Eppendorf Protein LoBind centrifuge tube at 13000 rpm (12641×*g*) for 23 min (MiniSpin Plus, Eppendorf, Hamburg, Germany). Supernatant was collected to quantify unadsorbed species. Batch adsorption samples for mixtures of BSA and NOM onto TiO_2 (0.5 g L^{-1}) were prepared following the same procedures, fixing the concentration of one species at 100 mg L^{-1} while the other was varied from (10 to 200) mg L^{-1}.

The adsorbed mass of BSA or NOM was determined by solution depletion, i.e., subtracting the remaining from the initial concentration, and dividing the depleted mass by the estimated TiO_2 surface area from the NIST CoA. BSA was quantified by the Bradford assay (SI);[64] for binary-

component solutions, corrections for interferences in the presence of NOM[65] were applied (Figure S1). NOM was analyzed by SEC with refractive index (RI) detection (method description in SI) to quantify solution depletion and identify adsorptive fractionation of NOM onto TiO_2. Spectral analysis of the NOM by batch- and SEC-UV-vis analysis[66-69] was also performed to evaluate adsorptive fractionation (SI).

Kinetic adsorption experiments

In situ ATR-FTIR spectroscopy was used to semi-quantitatively evaluate the kinetics of adsorption, displacement of adsorbed species, and multilayer adsorption processes. A Nicolet iS50 FTIR spectrometer (ThermoFisher Scientific, Waltham, MA) was equipped with a diamond/ZnSe single reflection ATR crystal (PIKE Technologies, Fitchburg, WI). Spectra were collected from (800 to 4000) cm^{-1} with a resolution of 2 cm^{-1} and averaged over 200 scans. 5 µL of TiO_2 (10 g L^{-1} in Milli-Q water) was dried onto the ATR crystal, and a flow cell (PIKE Technologies) was attached. Because the background solution chemistry and pH are important,[41, 70, 71] buffer solution with the same composition used in the adsorption experiments was flowed over the NPs to equilibrate the surface chemistry and also remove loosely attached NPs.

Adsorption experiments were conducted separately with pure NOM, pure BSA, or mixtures. For pure NOM or BSA, 100 mg L^{-1} solutions in the buffer were flowed over the NPs, and spectra were collected every 10 min and reprocessed using a background spectrum of macromolecule-free buffer over the TiO_2 film. We performed the same experiment for NOM-BSA mixtures (100 mg L^{-1} of each species), injected after ≈ 1 h mixing. To compare relative adsorbed amounts of NOM and BSA from the mixtures, spectra across (1300 to 1800) cm^{-1} were modeled as a linear combination of the single-component adsorbed NOM and BSA spectra to obtain fitted

coefficients, A'_{NOM} and A'_{BSA} (details in SI). For this analysis, 1800 cm^{-1} was largely free of NOM or BSA absorbance and selected as a base point to vertically align the spectra before fitting. The ATR-FTIR analysis is only semi-quantitative because of the variable TiO_2 film deposited between experiments; hence, fitted coefficients are not compared directly. Only ratios of coefficients, e.g. $\frac{A'_{\mathrm{BSA}}(t)}{A'_{\mathrm{NOM}}(t)}$, were compared between samples, normalizing the TiO_2 surface area and sample volume probed, roughly analogous to the use of internal standards for quantitative FTIR analysis.[72]

Sequential adsorption experiments were performed to evaluate interactions between adsorbed and dissolved macromolecules. Fresh TiO_2 NP films were prepared and equilibrated in buffer, followed by equilibration in NOM (100 mg L^{-1}), which was identified in batch experiments to preferentially adsorb. In one experiment, pure BSA (100 mg L^{-1}) was then injected over the NOM-coated TiO_2 to identify displacement or overcoating. In other experiments, a mixture of BSA and NOM was injected over the NOM-coated TiO_2, followed by a solution of pure BSA, to distinguish the role of solution-phase mixture interactions on BSA adsorption to NOM-coated TiO_2. Three mixtures were evaluated: BSA (50 mg L^{-1}) with NOM (100 mg L^{-1}), BSA (100 mg L^{-1}) with NOM (200 mg L^{-1}), and BSA (200 mg L^{-1}) with NOM (100 mg L^{-1}).

Results and Discussion

Batch single-component adsorption of BSA and NOM onto TiO_2 NPs

Batch adsorption experiments were performed at pH 7 to 7.5, where the TiO_2 NPs have a $|\zeta| < 20$ mV,[60, 73] and both BSA and NOM are negatively charged (isoelectric point of BSA ≈ 5.1;[74] zeta potential for NOM at pH 7 ≈ -40 mV).[35] The adsorption behavior will be determined by attractive forces, including Van der Waals forces, hydrophobic interactions, hydrogen bonding, and Ca^{2+} bridging in our media, as well as repulsive electrostatic and hydrophilic forces. While

uncoated TiO_2 NPs aggregate rapidly in this medium, increasing concentrations of BSA and NOM provided steric/electrosteric colloidal stability,[75, 76] as observed by DLS (Figure S4). Aggregation at lower adsorbate:NP ratios could reduce the available surface area for adsorption, but we obtained similar BSA adsorption isotherms at different TiO_2 concentrations, (0.5 and 1) g L^{-1}, suggesting the effect may be minimal. To obtain the entire isotherm with measurable solution concentrations, the initial concentrations of adsorbate used were higher than typical environmental concentrations, particularly for proteins which represent a small percent of dissolved organic carbon (DOC) in surface waters.[26, 77] However, the lower extent of our remaining (equilibrium) solution concentrations (≈ 4 mg L^{-1}) is within the range of higher concentrations observed (e.g. up to 40 mg L^{-1} of DOC in wetlands,[26] or (1 to 50) mg L^{-1} protein in urban watersheds and wastewater effluents[78-80]).

A Langmuir adsorption isotherm (Equation S2) was able to fit the single-component adsorption of BSA and NOM (Figure 1), with saturation adsorbed masses, q_{max}, of (2.6 and 0.90) mg m^{-2}, respectively, fitted by nonlinear regression. These values are higher than other reports, e.g. 1.7 mg m^{-2} for BSA at pH 7.3,[81] and ≈ 0.2 mg m^{-2} for NOM at pH 7,[24] and likely attributable to the presence of Ca^{2+} which enhances both albumin and NOM adsorption to TiO_2 by bridging.[82-85] Therefore, we caution extrapolation of results to media lacking Ca^{2+}. The Langmuir isotherm constant, K, for BSA (1.1 L mg^{-1}) was higher than that for NOM (0.051 L mg^{-1}). We interpret K only as an empirical fitting parameter indicative of the steeper slope of the BSA isotherm and also note wide 95% confidence intervals on the fitted K for BSA (Table S1).

We investigated the NOM adsorption in further detail, considering the heterogeneity of the NOM itself. Batch UV-vis absorbance data showed an increase in the spectral slope of the NOM remaining in solution after adsorption (Figure S5), indicative of preferential adsorption of higher

molar mass species with "activated" aromatic groups (i.e., those with polar ring substitutions, e.g., carbonyl, carboxyl, and ester groups).[68] The SEC analysis (Figure S3), along with providing adsorbed mass of NOM, confirmed preferential adsorption of higher molar mass NOM, consistent with prior studies.[18-20] The direct relationship between spectral slope and molar mass was also verified by SEC-UV-DAD analysis[67, 69] (Figure S6). Finally, ATR-FTIR analysis showed that the non-adsorbing, lower molar mass fraction contained higher amounts of functional groups at 1120 cm^{-1} (Figure S7), which are observed in hydrophilic NOM fractions and attributed to the C-O stretch of alcohol or carbohydrate species.[86, 87] The preferential adsorption was used to inform the properties of adsorbing NOM when parameterizing the competitive adsorption models hereafter.

Batch competitive adsorption from mixtures of NOM and BSA is kinetically-determined and monolayer-limited

Adsorption from mixtures of NOM and BSA onto TiO_2 was measured in two sets of batch experiments: varying the concentration of BSA in the presence of 100 mg L^{-1} NOM, and vice versa (Figure 1). NOM largely outcompetes BSA for adsorption, contrary to expectations from the single-component isotherms. To further explore this phenomenon, experimental observations were compared to two theoretical models: an equilibrium Langmuir adsorption model, and a kinetic adsorption model. Our goal is to identify a simple analytical model capable of describing the competitive adsorption when parameterized using only the single-component Langmuir parameters and known or measured properties of the macromolecules and NPs.

The competitive Langmuir adsorption model for *n* competing adsorbates is presented in Equation 1:[88]

$$q_i = \frac{q_{\max,i} K_i C_{\mathrm{f},i}}{1 + \sum_{j=1}^{n} (K_j C_{\mathrm{f},j})} \quad (1)$$

where q_i (mg m^{-2}) is the adsorbed mass of species i, and $C_{f,i}$ (mg L^{-1}) is the final solution concentration of i at the end of the adsorption experiment. $q_{max,i}$ (mg m^{-2}) and K_i (L mg^{-1}) are the maximum monolayer adsorbed capacity and the Langmuir isotherm constant, respectively, from each single-component isotherm. This equilibrium model was not capable of predicting adsorption from the mixtures (Figure 1), significantly overestimating the adsorbed mass of BSA relative to NOM. A key assumption of the Langmuir model is that adsorption is reversible, and compounds with higher affinity will displace others to achieve equilibrium. Contrarily, the observed data suggest that our system does not meet Langmuir assumptions.

The alternative limiting case is a kinetic adsorption model in which NOM and BSA adsorb *irreversibly*. Irreversible attachment has been modeled by random sequential adsorption (RSA) models[89, 90] or analogously by colloid deposition models.[91] For adsorption onto NPs in suspension, the depletion rate of adsorbate from solution, $\frac{dN_{\infty,i}}{dt}$, can be described by the Smoluchowski equation[92] with a dynamic site blocking function, $B(\theta)$:[91]

$$\frac{dN_{\infty,i}}{dt} = -\alpha\left[4\pi D(R_1 + R_2)N_{TiO_2}\right]N_{\infty,i}B(\theta) = -\alpha k_{f,i}N_{\infty,i}B(\theta) \quad (2)$$

where $N_{\infty,i}$ is the number concentration of macromolecules in bulk solution at time t, D is the summed diffusion coefficients for the macromolecule and NP, R_1 and R_2 are the hydrodynamic radii of the macromolecule and NP, N_{TiO_2} is the number concentration of TiO_2 NPs, α is the attachment efficiency, and θ represents the fractional surface coverage. The diffusion-limited rate coefficient for favorable attachment (no energy barrier) is represented by $k_{f,i}$. Notably, this model will always predict the same final surface coverage at infinite time, regardless of solution

concentration. Hence, this model is incapable of predicting the observed concentration-dependent single-component adsorption isotherms without incorporating additional conditions, such as spreading of macromolecules upon adsorption.[93, 94] The paradoxical nature of observing both irreversible and concentration-dependent adsorption has been discussed in the protein adsorption literature.[90, 95]

We do not propose to provide the most complete model to address this scenario but rather to obtain a simple kinetic model capable of explaining our experimental data on final adsorbed layer composition. We proceed by simplifying Equation 2 to eliminate the site-blocking function and assume favorable attachment (or equivalent attachment efficiencies for NOM and BSA). Incorporating site blocking requires a numerical solution and will not change the *final* adsorbed layer composition predicted, since the adsorption rates of all adsorbates are affected equally. Obtaining attachment efficiencies would require kinetic data or otherwise treatment of the attachment efficiencies as fitting parameters in the model.

For favorable attachment without site blocking, integrating Equation 2 yields Equation 3:

$$\ln\left(\frac{N_{\infty,i}}{N_{0,i}}\right) = -4\pi D(R_1 + R_2)N_{\mathrm{TiO_2}}t = -k_{f,i}t \quad (3)$$

where $N_{0,i}$ is the initial concentration of species i. The depleted concentration and adsorbed mass of each species at each time t is then obtained by a mass balance. Having eliminated the site blocking function, a stopping criterion is needed to end the adsorption of each species. In defining this criterion, we incorporate concentration-dependent adsorption (i.e. the possibility for undersaturation) by specifying that the adsorption of each species ends when it has reached

292 "equilibrium" with the surface sites that are unoccupied by the competing species *j*, as defined in
293 Equation 4:
294
295 $$q_i(t_{\text{stop},i}) = \frac{q_{\max,i} K_i C_i(t_{\text{stop},i})}{1 + K_i C_i(t_{\text{stop},i})} \left(1 - \sum_{j \neq i} \frac{q_j}{q_{\max,j}}\right) \quad (4)$$
296
297 In specifying $q_{\max,j}$ for the site depletion, we assume that the total available surface area
298 occupied at the saturation adsorbed mass is equivalent across all adsorbates. Equations 3 and 4 are
299 solved together to obtain different stopping times, $t_{\text{stop},i}$, for each adsorbate. Importantly, the
300 adsorption is made irreversible by holding the adsorbed mass of faster-adsorbing species fixed at
301 $q_i(t_{\text{stop},i})$ for all $t \geq t_{\text{stop},i}$. Thereafter, the slower-colliding species can continue adsorbing to any
302 remaining available sites until reaching its own stopping time. The final state is at disequilibrium
303 compared to Equation 1. Note that if the irreversibility criterion is eliminated and *q* and *C* are taken
304 at equilibrium, Equation 4 becomes equivalent to the competitive Langmuir model (Equation 1).
305 Overall, this kinetic model predicts the experimental data for the final adsorbed layer
306 composition significantly better than the equilibrium Langmuir model across all mixtures (Figure
307 1). The smaller size (higher diffusion coefficient) and higher number concentration of NOM
308 relative to BSA results in a higher adsorbed mass for NOM than predicted by the Langmuir
309 equilibrium model. Because of the high *K* parameter for BSA, the kinetic model predicts > 80%
310 overall surface saturation for any initial BSA concentration > 1 mg L^{-1} (in the presence of 100 mg
311 L^{-1} of NOM). The key assumptions of irreversible and monolayer-limited adsorption in this model
312 were then directly tested in ATR-FTIR experiments.
313
314 *Multilayers form upon sequential exposure of TiO_2 NPs to pure NOM and pure BSA*

In situ ATR-FTIR spectroscopy has previously been applied to evaluate the adsorption of BSA,[39, 41, 71, 96] NOM,[70] polymers,[97] and other compounds[98-100] onto TiO_2 and other surfaces.[100-103] This method allows semi-quantitative analysis of the kinetics and extent of adsorption onto NPs. First, individual spectra of adsorbed NOM or BSA were collected during adsorption to the TiO_2 NP film from 100 mg L^{-1} solutions (Figure S8). The strong peaks at (1410 and 1570) cm^{-1} for adsorbed NOM are likely attributable to deprotonated carboxyl groups ($–COO^-$)[104 105] and also include contributions from aliphatic hydrocarbons[87, 106] and aromatic alkenes,[87, 106] respectively, that absorb in these regions. Consistent with our batch fractionation results (Figure S7), the peak at 1125 cm^{-1} (C-O stretch of carbohydrates) in the < 10 kDa NOM fraction was not observed in the adsorbing NOM. For BSA, the two main peaks correspond to amide I at (1600 to 1700) cm^{-1} for C=O stretching, and amide II at (1500 to 1600) cm^{-1} for N-H bending and C-N stretching.[106,107]

Then, a sequential adsorption experiment was performed in which the surface of the deposited NPs was equilibrated with NOM (100 mg L^{-1}) as the kinetically-favored adsorbate, followed by pure BSA (100 mg L^{-1}). To quantify adsorption of multiple species, previous studies used peak heights when peaks did not overlap significantly for adsorbed protein[108] and other compounds.[46] Here, the broad bands for NOM and BSA overlap extensively, but peak locations did not shift significantly in mixed layers compared to the single-component adsorption. Hence, the mixed layer spectra were successfully modeled as a linear combination of the single-component adsorbed BSA and NOM spectra in the range of (1300 to 1800) cm^{-1} (Equation S6, Figure S9). The fitted coefficients, A'_{BSA} and A'_{NOM}, are only semi-quantitative but can be evaluated for trends in the adsorbed mass of each species within each experiment or when ratioed to normalize for TiO_2 surface or sample volume probed.

While in other cases, surface ligands with low affinity have been found to be displaced by higher affinity species,[106] results here agree with adsorption irreversibility: the adsorbed amount of NOM remained nearly constant during the subsequent adsorption of BSA (Figure S9). More notably, the extensive BSA adsorption suggests that pure BSA significantly overcoats adsorbed NOM, similar to other sequential adsorption experiments reporting multilayer formation of pure proteins onto humic-coated minerals.[43-45]

Comparing the batch (mixture) and *in situ* ATR-FTIR (sequential) adsorption, the formation of NOM-protein coronas on TiO_2 NPs then appears to be fundamentally different when the NPs are exposed to a mixture (monolayer restriction) *versus* sequential exposure to pure solutions (multilayer adsorption). To explain these contradictory behaviors, we hypothesize that intermolecular complexation between humic substances and proteins in solution, well-known to occur,[48-52] changes adsorption from mixtures compared to pure substances. Hence, we investigated the role of intermolecular interactions through additional SEC and *in situ* ATR-FTIR experiments.

Solution-phase complexation occurs between BSA and NOM

SEC experiments were performed to evaluate complexation interactions between NOM and BSA in the solution phase. BSA elutes from the SEC column from ≈ (11 to 18) min as two peaks, corresponding to BSA dimer and monomer, which were considered together in the analyses. NOM elutes primarily as a broad peak from ≈ (15 to 26) min. Upon increasing the ratio of NOM to BSA in solution, UV absorbance and RI in the BSA region increase significantly (Figure 2), indicating attachment of aromatic NOM species onto BSA. Complexation also quenches the BSA fluorescence, consistent with previous reports[109] and possibly indicative of binding of the NOM with fluorescent tryptophan residues in BSA or a change in BSA conformation. As with adsorption

360 to the TiO_2 NPs, NOM with higher molar masses have slightly higher affinity to complex with
361 BSA. The amount of NOM attached to the BSA estimated by SEC-RI analysis showed increasing
362 complexation with the ratio of NOM:BSA, and complexation was observed to proceed over ≈ 5 h
363 before equilibrating (Figure S10).
364
365 *Co-adsorption is followed by suppressed multilayer formation in simultaneous adsorption from*
366 *NOM-BSA mixtures onto TiO_2 NPs*
367 *In situ* ATR-FTIR was used to investigate the simultaneous adsorption of NOM and BSA
368 onto TiO_2 NPs and evaluate the effects of complexation in solution on the adsorption from NOM-
369 BSA mixtures onto TiO_2 NPs. First, simultaneous adsorption of BSA (100 mg L^{-1}) and NOM (100
370 mg L^{-1}) onto the *uncoated* TiO_2 was evaluated. While both species increasingly adsorb over time,
371 the ratio of adsorbed BSA to NOM decreases over the first hour (Figure 3). This trend can be
372 explained either by a lower affinity of BSA to adsorb upon complexation, or increasing co-
373 adsorption of NOM with BSA as it complexes to BSA over ≈ 5 h at the concentrations used here.
374 Batch adsorption experiments using isolated NOM-protein complexes suggested that
375 complexation does not largely suppress BSA adsorption onto *uncoated* TiO_2 (Figure S11); hence,
376 co-adsorption of NOM complexed with BSA may contribute more to the results observed in the
377 initial stage of adsorption to the uncoated TiO_2 NPs.
378 The larger picture from the mixture experiment is that the overall BSA adsorption does
379 indeed appear to be suppressed in the mixture relative to pure BSA: specifically, BSA adsorption
380 begins to plateau within 1 h in the mixture (Figure 4), but remains nearly linear over 1 h when
381 adsorbing from pure solution even after NOM has pre-adsorbed (Figure S9). We hypothesize that
382 over longer time scales, complexation of NOM onto dissolved BSA hinders the ability of BSA to

383 overcoat adsorbed layers *after* the TiO_2 surface has been saturated. To test this hypothesis,
384 adsorption from NOM-BSA mixtures onto NOM-coated TiO_2 NPs was evaluated (Figure 4 and
385 S12) and compared to subsequent adsorption of the pure BSA for various concentrations of BSA
386 and NOM. In all cases, after providing adequate opportunity for adsorption from the NOM-BSA
387 mixtures, subsequent injection of pure BSA led to further protein adsorption beyond that in the
388 mixtures. Hence, adsorption sites must be available to pure BSA that are not available to the
389 complexed BSA. We propose that the complexed BSA fills remaining bare TiO_2 sites (since NOM
390 is not completely saturated from 100 mg L^{-1} starting conditions), but has little affinity to overcoat
391 the adsorbed NOM after complexing with NOM in solution. On the contrary, the pure BSA is
392 capable to attach onto the adsorbed NOM to form an overcoating. While modeling this behavior
393 without more quantitative kinetic data is outside the scope of this study, possible extensions to the
394 kinetic model are discussed in the SI that could describe this multilayer formation.

395 In summary, the complexation interaction between NOM and BSA is a critical process
396 leading to the occurrence of fundamentally different adsorption phenomena under different NP
397 exposure conditions and time scales, as depicted in Figure 5. Multilayer formation occurs upon
398 sequential exposure to *pure* solutions of NOM and BSA. In mixtures, BSA-NOM complexes can
399 co-adsorb to the *uncoated* TiO_2 at short time scales. However, after the TiO_2 surface is saturated,
400 the complexation of NOM to BSA in solution ultimately hinders any further development of
401 NOM/protein multilayers on the TiO_2 NPs, such that monolayer restrictions are reasonable when
402 modeling batch adsorption from mixtures (Figure 1). Notably, in this system, all possible mixture
403 interactions (macromolecule–NP, macromolecule–macromolecule, and macromolecule–adsorbed
404 layer) and their kinetics are important.

405

406 *Implications*

407 This study has presented a thorough investigation of the fundamental mechanisms involved
408 in the competitive adsorption of NOM and proteins (with BSA as a model protein) onto TiO_2 NPs,
409 using both modeling and experimental methods to fully evaluate the adsorption process under a
410 range of possible NP exposure conditions. The behaviors observed here further expand our
411 understanding of the role of mixture interactions and kinetics on corona formation in
412 environmental media. Just as protein corona formation in biological systems is well known to be
413 a dynamic process, so will prediction of heterogeneous corona formation in environmental systems
414 require knowledge of not only the matrix and NP composition, but also the intermolecular
415 interactions in solution and at the NP surface, and the kinetics and history of these interactions.

416 To our knowledge, this study is the first to directly identify the roles of both dynamic
417 complexation in solution and the history of the NP surface on the competitive adsorption process
418 in environmental matrices containing mixtures of NOM and protein. The influence of sequential
419 exposure observed here will be most relevant during transport of NPs between environments, e.g.
420 from surface water to a biofilm layer concentrated in proteins, or bio-uptake, where an NOM-
421 coated NP can obtain a protein corona. Diurnal or seasonal patterns also produce fluctuations in
422 the composition of organic matter in natural and engineered water treatment systems.

423 Additional research is needed to evaluate generalizability from the single solution
424 chemistry and high adsorbate and NP concentrations in this study. The presence of Ca^{2+} in our
425 samples likely enhanced the adsorption of both proteins and NOM onto TiO_2, and hence the
426 adsorbed masses and adsorption irreversibility may change in media lacking Ca^{2+}. pH and ionic
427 strength also change the NP surface charge or screens charges, affecting adsorption. Using our

simple kinetic model to extrapolate to lower mixture concentrations (e.g. < 10 mg L^{-1} of both adsorbates), NOM is still predicted to outcompete such that the BSA adsorbed mass is relatively sensitive to the NOM concentration, whereas NOM adsorption is relatively insensitive to the presence of BSA. However, experiments are needed to confirm. Such studies should address whether long-term conditioning of NPs in lower, environmentally relevant macromolecule concentrations (but relatively high concentrations compared to relevant NP concentrations, i.e. minimal solution depletion) would result in similar adsorbed layers to those measured at high concentrations. True adsorption irreversibility would suggest that the final corona should not depend on absolute concentrations given sufficient time for adsorption.

We anticipate systematic investigations for mixtures of macromolecules covering a range of physicochemical properties (e.g., humic substances, proteins, polysaccharides, lipids, DNA, etc.) will enable elucidation of overarching rules to predict competitive adsorption onto NPs and other surfaces in complex environmental media. Future studies are needed to evaluate how the corona compositions and structures formed under different conditions will affect subsequent NP behavior in the environment. Most notably, we identified that exposure of the NP to a homogeneous mixture of NOM and proteins that have already undergone complexation will produce only a thin monolayer coating, whereas sequential or alternating exposures of the NP to different ratios of NOM and protein can result in multilayer coatings. The corona thickness and adsorbed mass are known to dominate the steric or electrosteric repulsion between NPs,[11, 110] and hence our study suggests that the details of the history of NP exposure to various macromolecules can be important to the overall fate and transport of the NPs. Corona composition, structure, and thickness are also likely to change the reactivity of NPs, including photoreactive TiO_2 NPs,[32-34] where the adsorbed macromolecules will interact with both organic pollutants and reactive oxygen

species. Finally, the degradation of the corona and transformation of the NP itself can also vary with corona composition, leading to longer-term differences in NP fate and transport.[111-113] The thoroughly characterized system presented here will be useful to investigate the effect of the composition and structure of NOM/protein coronas on the photoreactivity of TiO_2 NPs and reactive transformations of the corona.

ASSOCIATED CONTENT

Supporting Information

Experimental details, description of adsorption models, and additional complexation and adsorption experiments are provided. This information is available free of charge via the Internet at http://pubs.acs.org.

Notes

The authors declare no competing financial interest.

ACKNOWLEDGMENTS

This material is based upon work supported by the National Science Foundation under Grant No. 1705511. We gratefully acknowledge insightful comments from three anonymous reviewers that improved the quality of this research. We thank Prof. Michael Harold for use of the FTIR instrument, Dr. Vincent A. Hackley for the NIST SRM 1898 TiO_2 NPs, Prof. Gregory V. Lowry for the SEC column, Sergio De La Fuente for preliminary work in optimizing the Bradford assay, and Dr. Charisma Lattao for laboratory assistance.

References

1. Ju-Nam, Y.; Lead, J. R. Manufactured nanoparticles: An overview of their chemistry, interactions and potential environmental implications. *Sci. Total Environ.* **2008,** *400*, (1), 396-414.
2. Dwivedi, A. D.; Dubey, S. P.; Sillanpää, M.; Kwon, Y.-N.; Lee, C.; Varma, R. S. Fate of engineered nanoparticles: implications in the environment. *Coord. Chem. Rev.* **2015,** *287*, 64-78.
3. Wiesner, M. R.; Lowry, G. V.; Alvarez, P.; Dionysiou, D.; Biswas, P. Assessing the risks of manufactured nanomaterials. *Environ. Sci. Technol.* **2006,** *40*, (14), 4336-4345.
4. Louie, S. M.; Tilton, R. D.; Lowry, G. V. Critical review: impacts of macromolecular coatings on critical physicochemical processes controlling environmental fate of nanomaterials. *Environ. Sci. Nano* **2016,** *3*, (2), 283-310.
5. Philippe, A.; Schaumann, G. E. Interactions of dissolved organic matter with natural and engineered inorganic colloids: a review. *Environ. Sci. Technol.* **2014,** *48*, (16), 8946-62.
6. Grillo, R.; Rosa, A. H.; Fraceto, L. F. Engineered nanoparticles and organic matter: a review of the state-of-the-art. *Chemosphere* **2015,** *119*, 608-619.
7. Levard, C.; Hotze, E. M.; Lowry, G. V.; Brown Jr, G. E. Environmental transformations of silver nanoparticles: impact on stability and toxicity. *Environ. Sci. Technol.* **2012,** *46*, (13), 6900-6914.
8. Saptarshi, S. R.; Duschl, A.; Lopata, A. L. Interaction of nanoparticles with proteins: relation to bio-reactivity of the nanoparticle. *J. Nanobiotechnol.* **2013,** *11*, (1), 26.
9. Diegoli, S.; Manciulea, A. L.; Begum, S.; Jones, I. P.; Lead, J. R.; Preece, J. A. Interaction between manufactured gold nanoparticles and naturally occurring organic macromolecules. *Sci. Total Environ.* **2008,** *402*, (1), 51-61.
10. Surette, M. C.; Nason, J. A. Effects of surface coating character and interactions with natural organic matter on the colloidal stability of gold nanoparticles. *Environ. Sci. Nano* **2016,** *3*, (5), 1144-1152.
11. Petosa, A. R.; Jaisi, D. P.; Quevedo, I. R.; Elimelech, M.; Tufenkji, N. Aggregation and deposition of engineered nanomaterials in aquatic environments: Role of physicochemical interactions. *Environ. Sci. Technol.* **2010,** *44*, (17), 6532-6549.
12. Lin, S.; Mortimer, M.; Chen, R.; Kakinen, A.; Riviere, J. E.; Davis, T. P.; Ding, F.; Ke, P. C. NanoEHS beyond toxicity – focusing on biocorona. *Environ. Sci. Nano* **2017,** *4*, (7), 1433-1454.
13. Lynch, I.; Cedervall, T.; Lundqvist, M.; Cabaleiro-Lago, C.; Linse, S.; Dawson, K. A. The nanoparticle-protein complex as a biological entity; a complex fluids and surface science challenge for the 21st century. *Adv. Colloid Interface Sci.* **2007,** *134-135*, 167-74.
14. Moghimi, S. M.; Hunter, A. C.; Andresen, T. L. Factors controlling nanoparticle pharmacokinetics: an integrated analysis and perspective. *Annu. Rev. Pharmacol. Toxicol.* **2012,** *52*, 481-503.
15. Monopoli, M. P.; Aberg, C.; Salvati, A.; Dawson, K. A. Biomolecular coronas provide the biological identity of nanosized materials. *Nat. Nanotechnol.* **2012,** *7*, (12), 779-86.
16. Nel, A. E.; Madler, L.; Velegol, D.; Xia, T.; Hoek, E. M.; Somasundaran, P.; Klaessig, F.; Castranova, V.; Thompson, M. Understanding biophysicochemical interactions at the nano-bio interface. *Nat. Mater.* **2009,** *8*, (7), 543-57.
17. Walkey, C. D.; Chan, W. C. Understanding and controlling the interaction of nanomaterials with proteins in a physiological environment. *Chem. Soc. Rev.* **2012,** *41*, (7), 2780-99.

18. Li, Z.; Lowry, G. V.; Fan, J.; Liu, F.; Chen, J. High molecular weight components of natural organic matter preferentially adsorb onto nanoscale zero valent iron and magnetite. *Sci. Total Environ.* **2018,** *628-629*, 177-185.
19. Deonarine, A.; Lau, B. L.; Aiken, G. R.; Ryan, J. N.; Hsu-Kim, H. Effects of humic substances on precipitation and aggregation of zinc sulfide nanoparticles. *Environ. Sci. Technol.* **2011,** *45*, (8), 3217-23.
20. Hyung, H.; Kim, J.-H. Natural organic matter (NOM) adsorption to multi-walled carbon nanotubes: effect of NOM characteristics and water quality parameters. *Environ. Sci. Technol.* **2008,** *42*, (12), 4416-4421.
21. Baalousha, M.; Afshinnia, K.; Guo, L. Natural organic matter composition determines the molecular nature of silver nanomaterial-NOM corona. *Environ. Sci. Nano* **2018,** *5*, (4), 868-881.
22. Kang, S. H.; Xing, B. S. Humic acid fractionation upon sequential adsorption onto goethite. *Langmuir* **2008,** *24*, (6), 2525-2531.
23. Phong, D. D.; Hur, J. Using two-dimensional correlation size exclusion chromatography (2D-CoSEC) and EEM-PARAFAC to explore the heterogeneous adsorption behavior of humic substances on nanoparticles with respect to molecular sizes. *Environ. Sci. Technol.* **2018,** *52*, (2), 427-435.
24. Yang, K.; Lin, D.; Xing, B. Interactions of humic acid with nanosized inorganic oxides. *Langmuir* **2009,** *25*, (6), 3571-3576.
25. Artemyev, V. E., *Geochemistry of organic matter in river-sea systems*. Kluwer Academic Publishers: Dordrecht, The Netherlands, 1996.
26. Thurman, E. M., *Organic geochemistry of natural waters*. Kluwer Academic Publishers: Dordrecht, The Netherlands, 1987.
27. Carbonaro, S.; Sugihara, M. N.; Strathmann, T. J. Continuous-flow photocatalytic treatment of pharmaceutical micropollutants: Activity, inhibition, and deactivation of TiO_2 photocatalysts in wastewater effluent. *Appl. Catal., B* **2013,** *129*, 1-12.
28. Tan, W.; Peralta-Videa, J. R.; Gardea-Torresdey, J. L. Interaction of titanium dioxide nanoparticles with soil components and plants: current knowledge and future research needs – a critical review. *Environ. Sci. Nano* **2018,** *5*, (2), 257-278.
29. Lee, S.-Y.; Park, S.-J. TiO_2 photocatalyst for water treatment applications. *J. Ind. Eng. Chem.* **2013,** *19*, (6), 1761-1769.
30. Menard, A.; Drobne, D.; Jemec, A. Ecotoxicity of nanosized TiO_2. Review of in vivo data. *Environ. Pollut.* **2011,** *159*, (3), 677-84.
31. Curry, D. E.; Andrea, K. A.; Carrier, A. J.; Nganou, C.; Scheller, H.; Yang, D.; Youden, B.; Zhang, Y.; Nicholson, A.; Cui, S. Surface interaction of doxorubicin with anatase determines its photodegradation mechanism: insights into removal of waterborne pharmaceuticals by TiO_2 nanoparticles. *Environ. Sci. Nano* **2018,** *5*, (4), 1027-1035.
32. He, X.; Sanders, S.; Aker, W. G.; Lin, Y.; Douglas, J.; Hwang, H. M. Assessing the effects of surface-bound humic acid on the phototoxicity of anatase and rutile TiO_2 nanoparticles *in vitro*. *J. Environ. Sci.* **2016,** *42*, 50-60.
33. Li, Y.; Niu, J.; Shang, E.; Crittenden, J. C. Influence of dissolved organic matter on photogenerated reactive oxygen species and metal-oxide nanoparticle toxicity. *Water Res.* **2016,** *98*, 9-18.
34. Gao, X.; Zhou, K.; Zhang, L.; Yang, K.; Lin, D. Distinct effects of soluble and bound exopolymeric substances on algal bioaccumulation and toxicity of anatase and rutile TiO_2 nanoparticles. *Environ. Sci. Nano* **2018,** *5*, (3), 720-729.

35. Kim, J.; Shan, W.; Davies, S. H.; Baumann, M. J.; Masten, S. J.; Tarabara, V. V. Interactions of aqueous NOM with nanoscale TiO_2: Implications for ceramic membrane filtration-ozonation hybrid process. *Environ. Sci. Technol.* **2009,** *43*, (14), 5488-5494.
36. Chen, G.; Liu, X.; Su, C. Distinct effects of humic acid on transport and retention of TiO_2 rutile nanoparticles in saturated sand columns. *Environ. Sci. Technol.* **2012,** *46*, (13), 7142-7150.
37. Hotze, E. M.; Louie, S. M.; Lin, S.; Wiesner, M. R.; Lowry, G. V. Nanoparticle core properties affect attachment of macromolecule-coated nanoparticles to silica surfaces. *Environ. Chem.* **2014,** *11*, (3), 257-267.
38. Luo, M.; Huang, Y.; Zhu, M.; Tang, Y.-n.; Ren, T.; Ren, J.; Wang, H.; Li, F. Properties of different natural organic matter influence the adsorption and aggregation behavior of TiO2 nanoparticles. *J. Saudi Chem. Soc.* **2018,** *22*, (2), 146-154.
39. Bouhekka, A.; Bürgi, T. In situ ATR-IR spectroscopy study of adsorbed protein: Visible light denaturation of bovine serum albumin on TiO_2. *Appl. Surf. Sci.* **2012,** *261*, 369-374.
40. Kopac, T.; Bozgeyik, K.; Yener, J. Effect of pH and temperature on the adsorption of bovine serum albumin onto titanium dioxide. *Colloids Surf., A* **2008,** *322*, (1-3), 19-28.
41. Givens, B. E.; Xu, Z.; Fiegel, J.; Grassian, V. H. Bovine serum albumin adsorption on SiO_2 and TiO_2 nanoparticle surfaces at circumneutral and acidic pH: A tale of two nano-bio surface interactions. *J. Colloid Interface Sci.* **2017,** *493*, 334-341.
42. Kleber, M.; Sollins, P.; Sutton, R. A conceptual model of organo-mineral interactions in soils: self-assembly of organic molecular fragments into zonal structures on mineral surfaces. *Biogeochemistry* **2007,** *85*, (1), 9-24.
43. Pucci, A.; Paolo D'Acqui, L.; Calamai, L. Fate of prions in soil: interactions of RecPrP with organic matter of soil aggregates as revealed by LTA-PAS. *Environ. Sci. Technol.* **2008,** *42*, (3), 728-733.
44. Tan, W.; Norde, W.; Koopal, L. K. Interaction between lysozyme and humic acid in layer-by-layer assemblies: Effects of pH and ionic strength. *J. Colloid and Interface Sci.* **2014,** *430*, 40-46.
45. Sander, M.; Tomaszewski, J. E.; Madliger, M.; Schwarzenbach, R. P. Adsorption of insecticidal Cry1Ab protein to humic substances. 1. Experimental approach and mechanistic aspects. *Environ. Sci. Technol.* **2012,** *46*, (18), 9923-9931.
46. Schmidt, M. P.; Martinez, C. E. Supramolecular association impacts biomolecule adsorption onto goethite. *Environ. Sci. Technol.* **2018,** *52*, (7), 4079-4089.
47. Quiquampoix, H.; Burns, R. G. Interactions between proteins and soil mineral surfaces: environmental and health consequences. *Elements* **2007,** *3*, (6), 401-406.
48. Tan, W. F.; Koopal, L. K.; Weng, L. P.; van Riemsdijk, W. H.; Norde, W. Humic acid protein complexation. *Geochim. Cosmochim. Acta* **2008,** *72*, (8), 2090-2099.
49. Li, Y.; Tan, W.; Koopal, L. K.; Wang, M.; Liu, F.; Norde, W. Influence of soil humic and fulvic acid on the activity and stability of lysozyme and urease. *Environ. Sci. Technol.* **2013,** *47*, (10), 5050-5056.
50. Giachin, G.; Narkiewicz, J.; Scaini, D.; Ngoc, A. T.; Margon, A.; Sequi, P.; Leita, L.; Legname, G. Prion protein interaction with soil humic substances: environmental implications. *PloS One* **2014,** *9*, (6), e100016.
51. Tomaszewski, J. E.; Schwarzenbach, R. P.; Sander, M. Protein encapsulation by humic substances. *Environ. Sci. Technol.* **2011,** *45*, (14), 6003-6010.

52. Tan, W. F.; Koopal, L. K.; Norde, W. Interaction between humic acid and lysozyme, studied by dynamic light scattering and isothermal titration calorimetry. *Environ. Sci. Technol.* **2009,** *43*, (3), 591-596.
53. Smith, C. B.; Booth, C. J.; Wadzinski, T. J.; Legname, G.; Chappell, R.; Johnson, C. J.; Pedersen, J. A. Humic substances interfere with detection of pathogenic prion protein. *Soil Biol Biochem* **2014,** *68*, 309-316.
54. Hirsh, S. L.; McKenzie, D. R.; Nosworthy, N. J.; Denman, J. A.; Sezerman, O. U.; Bilek, M. M. The Vroman effect: competitive protein exchange with dynamic multilayer protein aggregates. *Colloids Surf., B* **2013,** *103*, 395-404.
55. Tsai, D. H.; Davila-Morris, M.; DelRio, F. W.; Guha, S.; Zachariah, M. R.; Hackley, V. A. Quantitative determination of competitive molecular adsorption on gold nanoparticles using attenuated total reflectance-Fourier transform infrared spectroscopy. *Langmuir* **2011,** *27*, (15), 9302-13.
56. Tsai, D. H.; Shelton, M. P.; DelRio, F. W.; Elzey, S.; Guha, S.; Zachariah, M. R.; Hackley, V. A. Quantifying dithiothreitol displacement of functional ligands from gold nanoparticles. *Anal. Bioanal. Chem.* **2012,** *404*, (10), 3015-23.
57. U.S. Environmental Protection Agency (EPA). *Methods for measuring the acute toxicity of effluents and receiving waters to freshwater and marine organisms*; Washington, DC, 2002.
58. Keller, A. A.; Wang, H.; Zhou, D.; Lenihan, H. S.; Cherr, G.; Cardinale, B. J.; Miller, R.; Ji, Z. Stability and aggregation of metal oxide nanoparticles in natural aqueous matrices. *Environ. Sci. Technol.* **2010,** *44*, (6), 1962-1967.
59. Taurozzi, J. S.; Hackley, V. A.; Wiesner, M. Preparation of nanoparticle dispersions from powdered material using ultrasonic disruption. *NIST Special Publication 1200* **2012**, (2), 1200-2.
60. National Institute of Standards and Technology (NIST). *Certificate of Analysis: SRM 1898 - Titanium dioxide nanomaterial*; Gaithersburg, MD, 2012.
61. Louie, S. M.; Spielman-Sun, E. R.; Small, M. J.; Tilton, R. D.; Lowry, G. V. Correlation of the physicochemical properties of natural organic matter samples from different sources to their effects on gold nanoparticle aggregation in monovalent electrolyte. *Environ. Sci. Technol.* **2015,** *49*, (4), 2188-2198.
62. Louie, S. M.; Tilton, R. D.; Lowry, G. V. Effects of molecular weight distribution and chemical properties of natural organic matter on gold nanoparticle aggregation. *Environ. Sci. Technol.* **2013,** *47*, (9), 4245-4254.
63. Roy, A. S.; Tripathy, D. R.; Chatterjee, A.; Dasgupta, S. A spectroscopic study of the interaction of the antioxidant naringin with bovine serum albumin. *J. Biophys. Chem.* **2010,** *1*, (03), 141.
64. Hammond, J. B.; Kruger, N. J., The Bradford method for protein quantitation. In *New Protein Techniques*, Humana Press: Clifton, NJ, 1988; pp 25-32.
65. Whiffen, L. K.; Midgley, D. J.; McGee, P. A. Polyphenolic compounds interfere with quantification of protein in soil extracts using the Bradford method. *Soil Biol. Biochem.* **2007,** *39*, (2), 691-694.
66. Bricaud, A.; Morel, A.; Prieur, L. Absorption by dissolved organic matter of the sea (yellow substance) in the UV and visible domains 1. *Limnol. Oceanogr.* **1981,** *26*, (1), 43-53.
67. Korshin, G.; Chow, C. W.; Fabris, R.; Drikas, M. Absorbance spectroscopy-based examination of effects of coagulation on the reactivity of fractions of natural organic matter with varying apparent molecular weights. *Water Res.* **2009,** *43*, (6), 1541-1548.

68. Korshin, G. V.; Li, C.-W.; Benjamin, M. M. Monitoring the properties of natural organic matter through UV spectroscopy: A consistent theory. *Water Res.* **1997,** *31*, (7), 1787-1795.
69. Yan, M.; Korshin, G.; Wang, D.; Cai, Z. Characterization of dissolved organic matter using high-performance liquid chromatography (HPLC)–size exclusion chromatography (SEC) with a multiple wavelength absorbance detector. *Chemosphere* **2012,** *87*, (8), 879-885.
70. Jayalath, S.; Wu, H.; Larsen, S. C.; Grassian, V. H. Surface adsorption of Suwannee River humic acid on TiO_2 nanoparticles: A study of pH and particle size. *Langmuir* **2018,** *34*, (9), 3136-3145.
71. Xu, Z.; Grassian, V. H. Bovine serum albumin adsorption on TiO_2 nanoparticle surfaces: Effects of pH and coadsorption of phosphate on protein–surface interactions and protein structure. *J. Phys. Chem. C* **2017,** *121*, (39), 21763-21771.
72. Bellamy, M. K. Using FTIR-ATR spectroscopy to teach the internal standard method. *J. Chem. Educ.* **2010,** *87*, (12), 1399-1401.
73. Taurozzi, J. S.; Hackley, V. A.; Wiesner, M. R. A standardised approach for the dispersion of titanium dioxide nanoparticles in biological media. *Nanotoxicology* **2013,** *7*, (4), 389-401.
74. Lee, W.-K.; Ko, J.-S.; Kim, H.-M. Effect of electrostatic interaction on the adsorption of globular proteins on octacalcium phosphate crystal film. *J. Colloid and Interface Sci.* **2002,** *246*, (1), 70-77.
75. Loosli, F.; Le Coustumer, P.; Stoll, S. TiO_2 nanoparticles aggregation and disaggregation in presence of alginate and Suwannee River humic acids. pH and concentration effects on nanoparticle stability. *Water Res.* **2013,** *47*, (16), 6052-6063.
76. Li, Y.; Yang, C.; Guo, X.; Dang, Z.; Li, X.; Zhang, Q. Effects of humic acids on the aggregation and sorption of nano-TiO_2. *Chemosphere* **2015,** *119*, 171-176.
77. Kawahigashi, M.; Kaiser, K.; Kalbitz, K.; Rodionov, A.; Guggenberger, G. Dissolved organic matter in small streams along a gradient from discontinuous to continuous permafrost. *Global Change Biol.* **2004,** *10*, (9), 1576-1586.
78. Westgate, P. J.; Park, C. Evaluation of proteins and organic nitrogen in wastewater treatment effluents. *Environ. Sci. Technol.* **2010,** *44*, (14), 5352-5357.
79. Aitkenhead-Peterson, J.; Steele, M.; Nahar, N.; Santhy, K. Dissolved organic carbon and nitrogen in urban and rural watersheds of south-central Texas: land use and land management influences. *Biogeochemistry* **2009,** *96*, (1-3), 119-129.
80. Sui, X.; Wu, Z.; Lin, C.; Zhou, S. Terrestrially derived glomalin-related soil protein quality as a potential ecological indicator in a peri-urban watershed. *Environ. Monit. Assess.* **2017,** *189*, (7), 315.
81. Giacomelli, C. E.; Avena, M. J.; De Pauli, C. P. Adsorption of bovine serum albumin onto TiO_2 particles. *J. Colloid and Interface Sci.* **1997,** *188*, (2), 387-395.
82. Kim, J.; Shan, W.; Davies, S. H. R.; Baumann, M. J.; Masten, S. J.; Tarabara, V. V. Interactions of aqueous NOM with nanoscale TiO_2: Implications for ceramic membrane filtration-ozonation hybrid process. *Environ. Sci. Technol.* **2009,** *43*, (14), 5488-5494.
83. Ellingsen, J. E. A study on the mechanism of protein adsorption to TiO2. *Biomaterials* **1991,** *12*, (6), 593-596.
84. Klinger, A.; Steinberg, D.; Kohavi, D.; Sela, M. N. Mechanism of adsorption of human albumin to titanium in vitro. *J. Biomed. Mater. Res.* **1998,** *36*, (3), 387-392.
85. Wassell, D. T. H.; Embery, G. Adsorption of bovine serum albumin on to titanium powder. *Biomaterials* **1996,** *17*, (9), 859-864.

86. Senesi, N.; Miano, T.; Provenzano, M.; Brunetti, G. Spectroscopic and compositional comparative characterization of IHSS reference and standard fulvic and humic acids of various origin. *Sci. Total Environ.* **1989,** *81*, 143-156.
87. Croue, J.-P.; Korshin, G. V.; Benjamin, M. M., *Characterization of natural organic matter in drinking water*. American Water Works Association: 2000.
88. Rouquerol, J.; Rouquerol, F.; Sing, K. S.; Llewellyn, P.; Maurin, G., *Adsorption by powders and porous solids: Principles, methodology and applications*. 2nd ed.; Academic Press: Amsterdam, The Netherlands, 2012.
89. Evans, J. W. Random and cooperative sequential adsorption. *Rev. Mod. Phys.* **1993,** *65*, (4), 1281-1329.
90. Rabe, M.; Verdes, D.; Seeger, S. Understanding protein adsorption phenomena at solid surfaces. *Adv. Colloid Interface Sci.* **2011,** *162*, (1-2), 87-106.
91. Johnson, P. R.; Elimelech, M. Dynamics of colloid deposition in porous media: Blocking based on random sequential adsorption. *Langmuir* **1995,** *11*, (3), 801-812.
92. Hiemenz, P. C.; Rajagopalan, R., *Principles of colloid and surface chemistry*. 3rd ed.; CRC Press: Boca Raton, FL, 1997.
93. Van Tassel, P. R.; Guemouri, L. l.; Ramsden, J. J.; Tarjus, G.; Viot, P.; Talbot, J. A particle-level model of irreversible protein adsorption with a postadsorption transition. *J. Colloid and Interface Sci.* **1998,** *207*, (2), 317-323.
94. Van Tassel, P. R.; Viot, P.; Tarjus, G.; Talbot, J. Irreversible adsorption of macromolecules at a liquid–solid interface: Theoretical studies of the effects of conformational change. *J. Phys. Chem.* **1994,** *101*, (8), 7064-7073.
95. Ramsden, J. J. Puzzles and paradoxes in protein adsorption. *Chem. Soc. Rev.* **1995,** *24*, (1), 73-78.
96. Mudunkotuwa, I. A.; Al Minshid, A.; Grassian, V. H. ATR-FTIR spectroscopy as a tool to probe surface adsorption on nanoparticles at the liquid–solid interface in environmentally and biologically relevant media. *Analyst* **2014,** *139*, (5), 870-881.
97. Adeleye, A. S.; Keller, A. A. Interactions between algal extracellular polymeric substances and commercial TiO_2 nanoparticles in aqueous media. *Environ. Sci. Technol.* **2016,** *50*, (22), 12258-12265.
98. Hase, M.; Scheffelmaier, R.; Hayden, S.; Rivera, D. Quantitative *in situ* attenuated total internal reflection Fourier transform infrared study of the isotherms of poly (sodium 4-styrene sulfonate) adsorption to a TiO_2 surface over a range of cetylpyridinium bromide monohydrate concentration. *Langmuir* **2010,** *26*, (8), 5534-5543.
99. Mudunkotuwa, I. A.; Grassian, V. H. Citric acid adsorption on TiO_2 nanoparticles in aqueous suspensions at acidic and circumneutral pH: surface coverage, surface speciation, and its impact on nanoparticle− nanoparticle interactions. *J. Am. Chem. Soc.* **2010,** *132*, (42), 14986-14994.
100. Pettibone, J. M.; Cwiertny, D. M.; Scherer, M.; Grassian, V. H. Adsorption of organic acids on TiO_2 nanoparticles: effects of pH, nanoparticle size, and nanoparticle aggregation. *Langmuir* **2008,** *24*, (13), 6659-6667.
101. Liang, L.; Luo, L.; Zhang, S. Adsorption and desorption of humic and fulvic acids on SiO_2 particles at nano-and micro-scales. *Colloids Surf., A* **2011,** *384*, (1-3), 126-130.
102. Das, K.; Kundu, S. Adsorption and conformation variation of BSA protein with the size variation of the metallic nanoparticles in LB film. *Colloids Surf., A* **2015,** *468*, 56-61.

103. Jeyachandran, Y.; Mielczarski, E.; Rai, B.; Mielczarski, J. Quantitative and qualitative evaluation of adsorption/desorption of bovine serum albumin on hydrophilic and hydrophobic surfaces. *Langmuir* **2009,** *25*, (19), 11614-11620.
104. Max, J.-J.; Chapados, C. Infrared spectroscopy of aqueous carboxylic acids: comparison between different acids and their salts. *J. Phys. Chem. A* **2004,** *108*, (16), 3324-3337.
105. Francioso, O.; Sanchez-Cortes, S.; Tugnoli, V.; Ciavatta, C.; Sitti, L.; Gessa, C. Infrared, Raman, and nuclear magnetic resonance (^{1}H, ^{13}C, and ^{31}P) spectroscopy in the study of fractions of peat humic acids. *Appl. Spectrosc.* **1996,** *50*, (9), 1165-1174.
106. Mudunkotuwa, I. A.; Grassian, V. H. Biological and environmental media control oxide nanoparticle surface composition: the roles of biological components (proteins and amino acids), inorganic oxyanions and humic acid. *Environ. Sci. Nano* **2015,** *2*, (5), 429-439.
107. Tsai, D.-H.; DelRio, F. W.; Keene, A. M.; Tyner, K. M.; MacCuspie, R. I.; Cho, T. J.; Zachariah, M. R.; Hackley, V. A. Adsorption and conformation of serum albumin protein on gold nanoparticles investigated using dimensional measurements and *in situ* spectroscopic methods. *Langmuir* **2011,** *27*, (6), 2464-2477.
108. Chittur, K. K. FTIR/ATR for protein adsorption to biomaterial surfaces. *Biomaterials* **1998,** *19*, (4-5), 357-369.
109. Wang, Z.; Cao, J.; Meng, F. Interactions between protein-like and humic-like components in dissolved organic matter revealed by fluorescence quenching. *Water Res.* **2015,** *68*, 404-413.
110. Phenrat, T.; Song, J. E.; Cisneros, C. M.; Schoenfelder, D. P.; Tilton, R. D.; Lowry, G. V. Estimating attachment of nano- and submicrometer-particles coated with organic macromolecules in porous media: Development of an empirical model. *Environ. Sci. Technol.* **2010,** *44*, (12), 4531-4538.
111. Louie, S. M.; Gorham, J. M.; McGivney, E. A.; Liu, J. Y.; Gregory, K. B.; Hackley, V. A. Photochemical transformations of thiolated polyethylene glycol coatings on gold nanoparticles. *Environ. Sci. Nano* **2016,** *3*, (5), 1090-1102.
112. Louie, S. M.; Gorham, J. M.; Tan, J. J.; Hackley, V. A. Ultraviolet photo-oxidation of polyvinylpyrrolidone (PVP) coatings on gold nanoparticles. *Environ. Sci. Nano* **2017,** *4*, (9), 1866-1875.
113. Nguyen, M. L.; Murphy, J. A.; Hamlet, L. C.; Lau, B. L. T. Ligand-dependent Ag_2S formation: changes in deposition of silver nanoparticles with sulfidation. *Environ. Sci. Nano* **2018,** *5*, (5), 1090-1095.

Figures

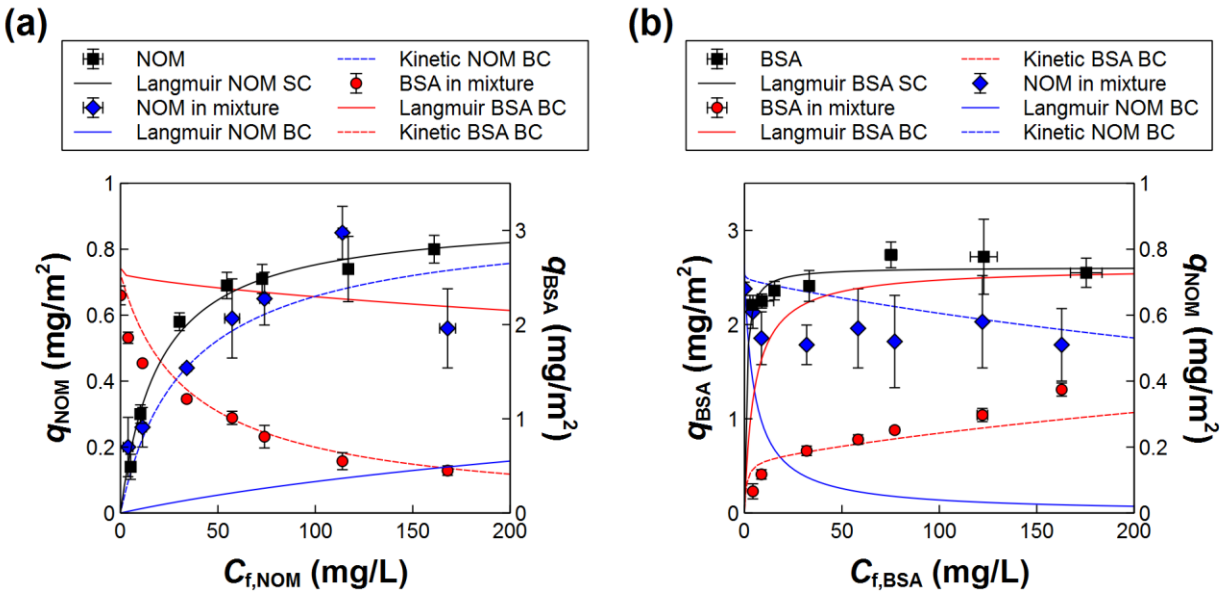

Figure 1. Batch adsorption isotherms onto TiO_2 NPs for (a) the single-component (SC) solution of NOM and binary-component (BC) mixtures of NOM with a fixed initial concentration of BSA (100 mg L^{-1}), and (b) the SC solution of BSA and BC mixtures of BSA with a fixed initial concentration of NOM (100 mg L^{-1}). Isotherms were collected on 500 mg L^{-1} TiO_2 NPs in a background of 1.2 mM $NaHCO_3$ and 0.85 mM $CaCl_2$ (pH 7 to 7.5). Solid and dashed lines represent the Langmuir and kinetic models, respectively. Error bars represent the standard deviation of n = 3 samples.

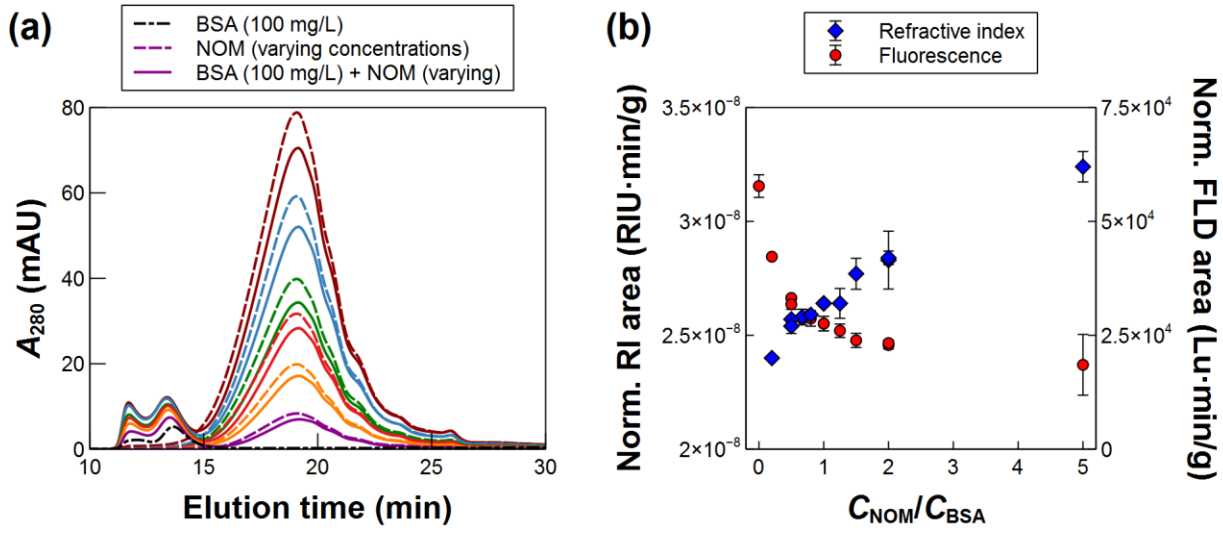

780

Figure 2. SEC-UV_{280} chromatograms for BSA-NOM mixtures (a) were collected for BSA (100 mg L^{-1}), NOM (20, 50, 80, 100, 150, and 200 mg L^{-1}, from lower to higher UV absorbances), and their mixtures. For the BSA peaks, along with the increase in UV absorbance upon NOM complexation, addition of NOM mass onto the BSA can be identified by RI detection and quenching of the BSA fluorescence (b). Peak areas in (b) are normalized by the injected BSA mass. All samples were prepared in a buffer of 1.2 mM $NaHCO_3$ with 0.85 mM $CaCl_2$ (pH 7), then measured in an SEC mobile phase of 4 mM phosphate with 25 mM NaCl (pH 7) to avoid SEC column fouling by NOM in Ca^{2+}-containing medium (SI). Additional data were also collected for mixtures of 100 mg L^{-1} NOM with varying BSA (not shown). Error bars represent the standard deviation of $n = 2$ independently prepared samples.

781

782

783

784

785

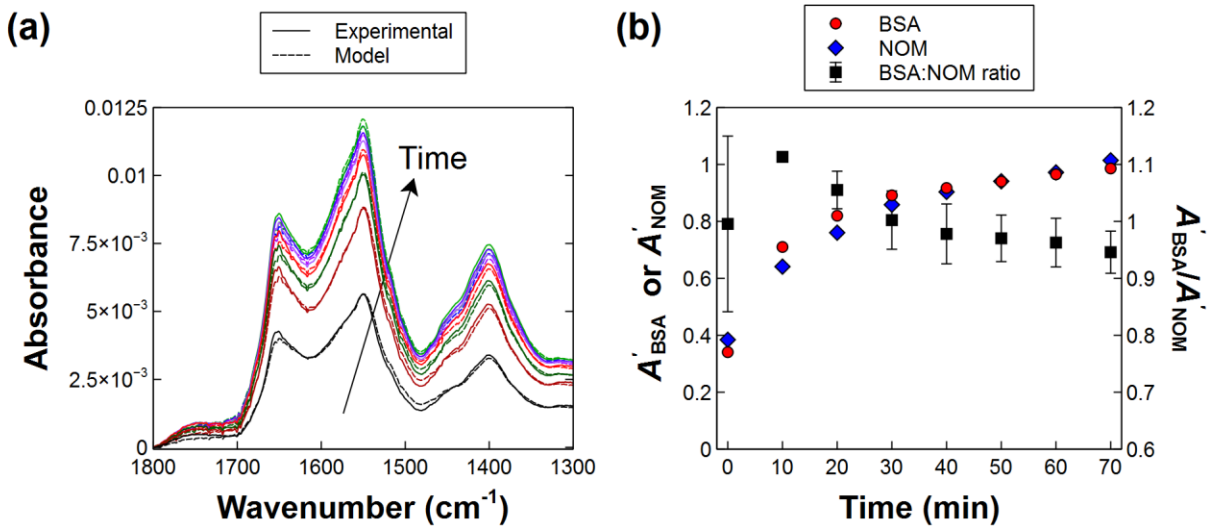

786

Figure 3. *In situ* ATR-FTIR experiment for simultaneous adsorption from mixtures of BSA (100 mg L^{-1}) and NOM (100 mg L^{-1}) onto TiO_2 NPs in the same buffer as the batch adsorption experiments. The mixture was prepared immediately before injecting. (a) The measured spectra (solid lines) in the range of (1300 to 1800) cm^{-1} were modeled as a linear combination of the spectra for pure BSA and pure NOM (dashed lines). (b) Fitted adsorbed amounts (*A*') of BSA and NOM both increase over time, while the relative ratio of BSA:NOM decreases. Ratios plotted represent the average ± standard deviation of the ratios determined at each time point within each of $n = 2$ independent experiments.

787

788

789

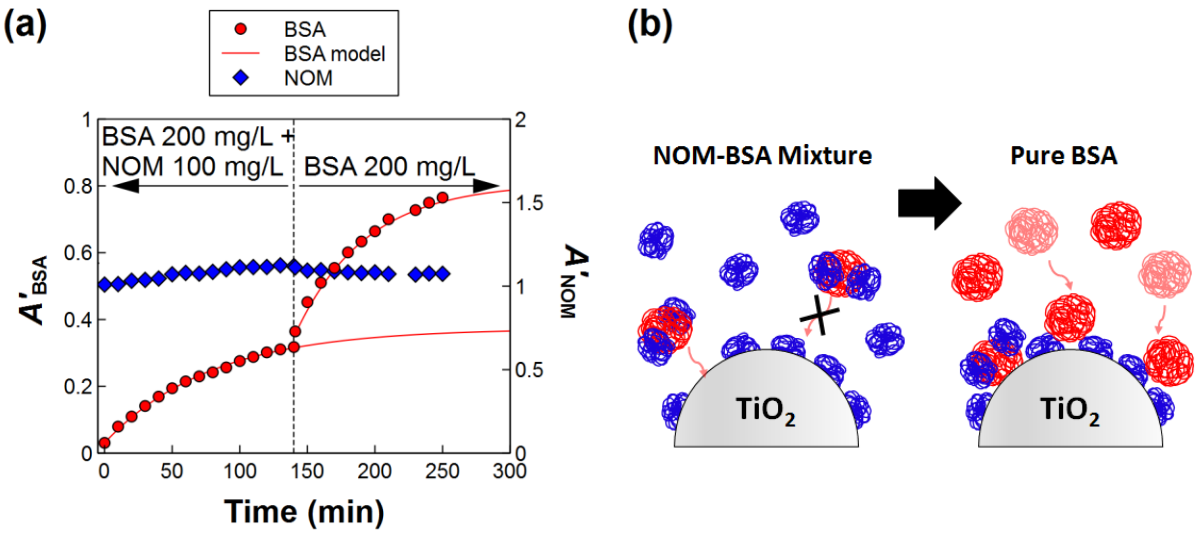

790

Figure 4. *In situ* ATR-FTIR experiment for the sequential adsorption of a mixture of BSA and NOM, followed by pure BSA, onto NOM-coated TiO_2 NPs. The initial NOM layer was pre-adsorbed from a 100 mg L^{-1} solution. Adsorption coefficients (*A*') were fitted as described in the SI. After the adsorption of complexed BSA from a mixture with NOM, additional protein is able to adsorb readily from a pure BSA solution. Similar results were obtained in replicate experiments. Considering the results of other combinations of concentrations (Figure S12), the conceptual model in (b) is proposed where complexed BSA fills any vacant sites on the TiO_2 surface, but multilayer formation is strongly suppressed relative to pure BSA.

791

792

793

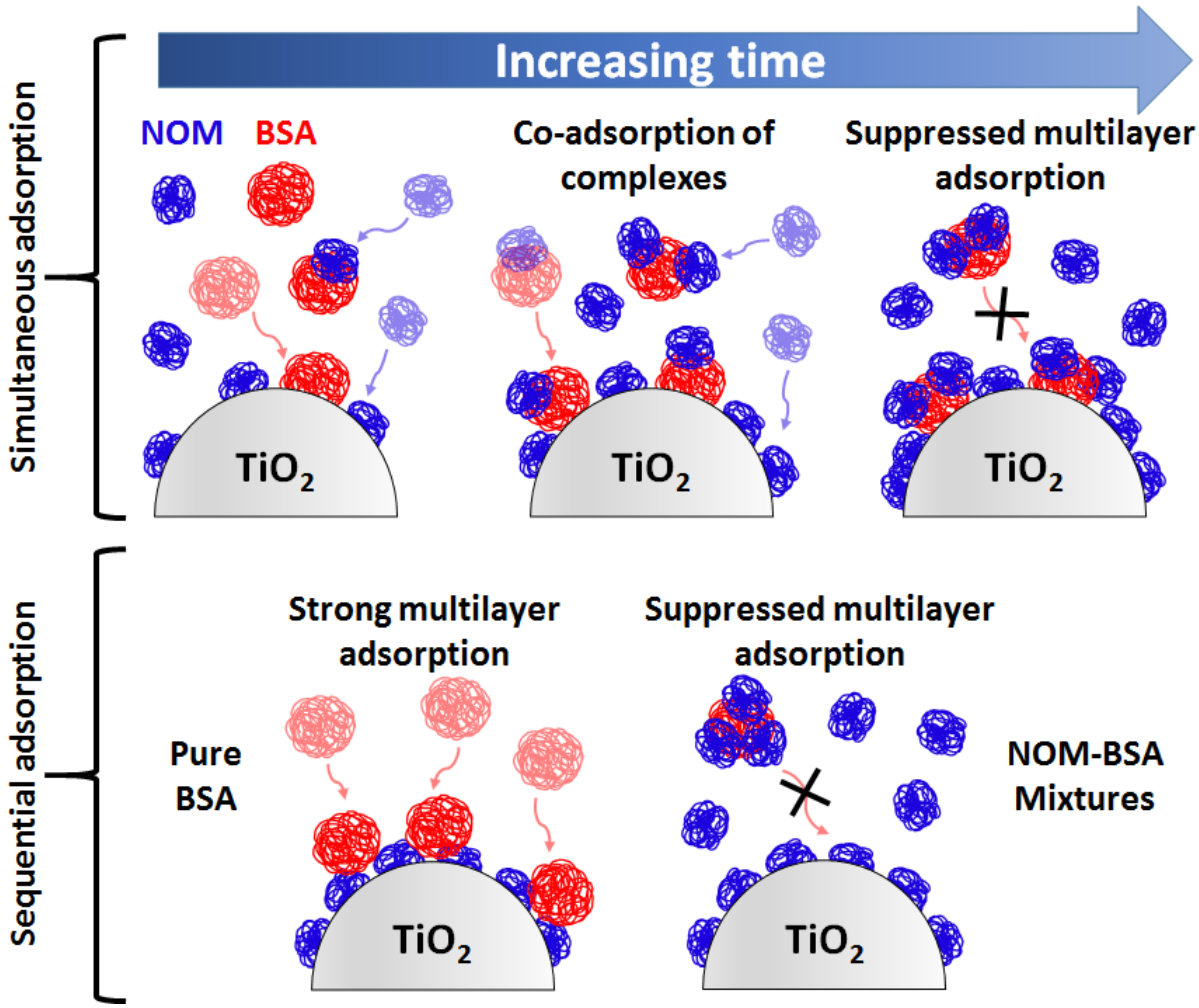

794

Figure 5. Conceptual model for competitive adsorption of NOM and BSA onto TiO_2 NPs, accounting for the critical role of dynamic intermolecular interactions. In simultaneous adsorption experiments (top), complexation of NOM to BSA initially results in co-adsorption to the uncoated TiO_2; however, complexation also hinders any subsequent multilayer adsorption after the TiO_2 surface is saturated. Sequential adsorption experiments (bottom) further demonstrated that pure protein readily overcoats NOM, whereas the multilayer adsorption is suppressed upon complexation of NOM to BSA.

795

796

797